Pergamon

Int. J. Heat Mass Transfer. Vol. 37, Suppl. 1, pp. 265–272, 1994

0017-9310/94 $6.00+0.00

0017-9310(93)E0082-R

Vaporization of a binary unsteady spray at high temperature and high pressure

M. KLINGSPORN and U. RENZ

Lehrstuhl für Wärmeübertragung und Klimatechnik, RWTH Aachen, 52056 Aachen, Germany

Abstract—A numerical model has been formulated for a binary droplet spray evaporating under diesel engine conditions. The liquid phase model considers the transport processes of heat conduction and species diffusion and includes variable property effects. The gaseous phase is described by the conservation equations for momentum, energy and species for unsteady, turbulent flows. The solution procedure is based on an Eulerian gas and a Lagrangian drop formulation. It is shown that for spray conditions, characterized by droplets with mean sizes of 20 μm and inlet velocities in the range of 200 m s^{-1}, and by a gaseous atmosphere at a temperature of 500°C and a pressure of 45 bar, the influence of the diffusive transport processes within the droplet cannot be neglected. The numerical model was used to predict the vaporization rate of *n*-heptane/*n*-decane sprays.

1. INTRODUCTION

MANY THEORETICAL and experimental investigations have been carried out in the past years to increase the fundamental understanding of vaporization and combustion of liquid fuels. Detailed discussions on the subject can be found in the review articles by Faeth [1], Sirignano [2], and Law [3]. Most of the work was either concentrated on single droplets or on droplets in steady sprays.

Numerical simulation procedures for transient sprays, such as diesel sprays in rather comprehensive codes developed for engine design, are normally based on an Eulerian gas and a Lagrangian drop formulation. Examples of such codes developed for engine design can be found in refs. [4] and [5]. Due to the limited computer storage and computing time for real three-dimensional problems the spray formulation in those codes is simplified. Empirical relations are used for the atomization of the liquid into droplets near the injection nozzle [6–8]. The momentum, energy, and mass transfer between the liquid and the gaseous phase is based on well known relations for drag coefficients, Nusselt and Sherwood numbers of single solid spheres. Although a number of papers have been published recently dealing with vaporization of binary droplets [9–14] it is assumed that diesel can be approximated by a one-component liquid.

In this work the vaporization of a binary fuel spray under diesel like conditions was investigated, taking into account the effects of variable properties of the liquid, of heat conduction and species diffusion within the droplet.

2. MODEL FORMULATION

A schematic view of the physical situation of the problem is shown in Fig. 1. A given amount of fuel is injected through the hole of the injection nozzle to the high temperature and high pressure gas in the cylinder, during an injection time of typically 2 ms. The gas is accelerated and cooled down by the evaporating droplet spray. The transient spray phenomena can be divided in the following submodels: nozzle flow, atomization, break up (including collision and coagulation in the near nozzle region), interphase heat, mass, and momentum transfer from the droplets to the surrounding gas, ignition and eventually combustion of the vapour phase.

The fuel rate history depends on the injection pressure, needle lift, etc. and can normally be evaluated experimentally. The flow inside the nozzle hole and the resulting velocity of the exiting two-phase flow is influenced by cavitation effects in the nozzle. Complex

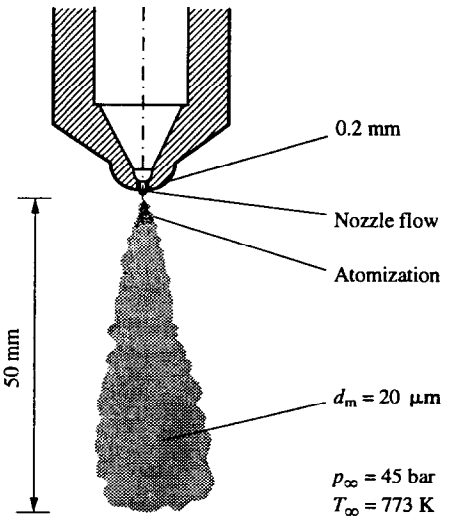

FIG. 1. A schematic view of the problem.

NOMENCLATURE

B	mass transfer number	t	time [s]
C_D	drag coefficient	T	temperature [K]
c_p	specific heat [J kg^{-1} K^{-1}]	u	velocity [m s^{-1}].
d_d	droplet diameter [m]		
D	diffusion coefficient [m^2 s^{-1}]	Greek symbols	
h	heat transfer coefficient [W m^{-2} K^{-1}]	α	thermal diffusivity, $k/\rho c_p$
k	thermal conductivity [W m^{-1} K^{-1}]	ε_i	partial vaporization rate, $\dot{m}_i/\dot{m}$
K	correction for density ratio	μ	dynamic viscosity [kg m^{-1} s^{-1}]
L	latent heat of vaporization [J kg^{-1}]	ξ	mass fraction
$\dot{m}$	vaporization rate [kg s^{-1}]	ρ	density [kg m^{-3}].
Nu	Nusselt number		
Pr	Prandtl number, μ/kc_p	Subscripts	
$\dot{Q}_{conv}$	convectional heat flow rate [W]	d	droplet
$\dot{Q}_{vap}$	latent heat flow rate [W]	g	gas phase
Re	Reynolds number	i	component
r	radial coordinate [m]	s	surface
r_d	droplet radius [m]	V	vapour
Sc	Schmidt number, $\mu/\rho D$	0	initial value
Sh	Sherwood number	∞	free-stream condition.

submodels on cavitating nozzle flows [6] or atomization, collision and coagulation processes [7, 8] are known from literature, but they need further validation by experiments. They are not considered in the present work. An initial droplet size distribution and a visually observed spray angle have been used instead, as a boundary condition at the nozzle exit. Since ignition and combustion are not predominant during the first millisecond, these effects can be ignored at this stage. The main emphasis of the work presented here is on the influence of the variable properties and the diffusional processes of heat and mass within the droplets on the vaporization rate of a binary fuel at high temperature and pressure.

3. GOVERNING EQUATIONS

3.1. *Liquid phase*

Neglecting internal convection, interdiffusion and radiation and assuming spherical symmetry, the energy and species conservation equations for a binary droplet with variable properties can be written as follows (see Kneer *et al.* [9]):

Energy:

$$\frac{\partial T_d}{\partial t} = \alpha_d\left[\frac{\partial^2 T_d}{\partial r^2} + \left(\frac{2}{r} + \frac{1}{k_d}\frac{\partial k_d}{\partial r}\right)\frac{\partial T_d}{\partial r}\right]. \quad (1)$$

Species conservation:

$$\frac{\partial \xi_{i,d}}{\partial t} = D_{AB}\left[\frac{\partial^2 \xi_{i,d}}{\partial r^2} + \left(\frac{2}{r} + \frac{1}{\rho_d}\frac{\partial \rho_d}{\partial r} + \frac{1}{D_{AB}}\frac{\partial D_{AB}}{\partial r}\right)\frac{\partial \xi_{i,d}}{\partial r}\right] - \xi_{i,d}\frac{1}{\rho_d}\frac{\partial \rho_d}{\partial t}. \quad (2)$$

Boundary conditions at the centre and at the surface are as follows:

$$r = 0: \quad \frac{\partial T_d}{\partial r} = 0; \quad \frac{\partial \xi_{i,d}}{\partial r} = 0 \quad (3)$$

$$r = r_d(t): \quad 4\pi r_d^2 k_d \frac{\partial T}{\partial r} = \dot{Q}_{conv} - \dot{Q}_{vap} \quad (4)$$

$$\rho_d D_{AB}\frac{\partial \xi_{i,d}}{\partial r} = \frac{\dot{m}}{4\pi r_d^2}(\xi_{i,d,s} - \varepsilon_i). \quad (5)$$

$\dot{Q}_{conv}$ represents the convective heat transfer from the gas to the surface

$$\dot{Q}_{conv} = 4\pi r_d^2 h(T_{g,\infty} - T_{g,s}). \quad (6)$$

The heat transfer coefficient h is evaluated using an empirical Nusselt formula for spheres

$$h = \frac{f k_g Nu}{d_d(e^f - 1)} \quad (7)$$

with

$$f = \frac{c_{p,V}\rho_g D_g \ln(1+B)}{k_g} \quad (8)$$

$$B = \frac{\sum_{i=1}^{2}\xi_{i,g,s} - \sum_{i=1}^{2}\xi_{i,g,\infty}}{1 - \sum_{i=1}^{2}\xi_{i,g,s}} \quad (9)$$

$$Nu = 2 + 0.6\,Re^{0.5}\,Pr^{1/3}. \quad (10)$$

The vapour mass fractions at the surface are calculated using Raoults law assuming ideal mixing behaviour. $\dot{Q}_{vap}$ is the contribution of the evaporated mass to the energy balance and $\dot{m}$ the appropriate mass transferred

$$\dot{Q}_{\text{vap}} = \sum_{i=1}^{2} \dot{m}_i L_i. \tag{11}$$

The total mass flow is

$$\dot{m} = \rho_g D_g \pi d_d Sh \ln(1+B) \tag{12}$$

with the Sherwood number

$$Sh = 2 + 0.6\, Re^{0.5}\, Sc^{1/3}. \tag{13}$$

The actual drop diameter is obtained from the liquid phase mass balance

$$\frac{dr_d}{dt} = -\frac{1}{\rho_d(r_d,t) r_d^2}\left(\frac{\dot{m}}{4\pi} + \int_0^{r_d(t)} \frac{\partial \rho_d}{\partial t} r^2\, dr\right). \tag{14}$$

The momentum transfer from the droplet to the gas is described by an empirical drag law valid for spherical particles. The velocity decrease of the injected droplets is calculated from

$$\frac{du_d}{dt} = \frac{3}{4}\frac{\mu_\infty}{\rho_d d_d^2} Re\, C_D \frac{|u_g - u_d|}{K} \tag{15}$$

with

$$C_D = \frac{24}{Re}(1 + 0.15\, Re^{0.687}) \tag{16}$$

and

$$K = 1 - 0.5\frac{\rho_\infty}{\rho_d}. \tag{17}$$

3.2. *Gaseous phase*

Two models will be presented for the gaseous phase. The first one, which will be used to discuss the effects of the extended droplet model, assumes a large hot environment at rest. The gaseous phase is not influenced by the evaporating droplet. In the second model a transient fuel spray is injected into a limited gas volume of a cylinder. In that case momentum, heat and mass is transferred to the gas, changing its velocity, temperature and vapour mass fraction fields. The unsteady, turbulent conservation equations for mass, momentum, energy and species concentration have to be solved in addition to the liquid phase conservation equations. The gas phase equations can be written in a general form as follows

$$\frac{\partial}{\partial t}(\rho\phi) + \frac{\partial}{\partial x}(\rho u \phi) + \frac{1}{r}\frac{\partial}{\partial r}(r \rho v \phi) = \frac{\partial}{\partial x}\left(\Gamma_\phi \frac{\partial \phi}{\partial x}\right) + \frac{1}{r}\frac{\partial}{\partial r}\left(r \Gamma_\phi \frac{\partial \phi}{\partial r}\right) + S_\phi \tag{18}$$

where the general variable ϕ means velocity component u, v, total enthalpy h_t, species ξ_1 and ξ_2 for the fuel components and ξ_3 for the ambient gas, and the turbulence quantities k and ε. The source terms include the contributions of momentum, energy and mass transferred from the liquid phase.

Since a single spray in an axisymmetric pressure chamber is under investigation a cylindrical coordinate system has been chosen.

For the liquid phase a mixture of *n*-heptane and *n*-decane was chosen. The ambient gas was air. The properties of both phases are tabulated in the Appendix.

4. SOLUTION PROCEDURE

4.1. *Liquid phase*

The temperature and the species concentration within the droplet were evaluated by an implicit numerical solution of the discretized conservation equations. Following Kneer *et al.* [9] a non-dimensionalized spatial coordinate with ten evenly distributed grid points was used. This grid size is a fair compromise between accuracy and computational effort for the coupled systems of the conservation equations.

4.2. *Gaseous phase*

The gas phase calculations were performed with a modified version of the finite volume code FLUENT [15], which was extended for the droplet phase to take transient sprays of binary liquids with variable properties into account. A computational grid of 60 by 30 lines was chosen. The time increment was 0.01 ms.

4.3. *Initial and boundary conditions*

The transient injection rate was taken from measurements. The total injected fuel mass is represented by 50 droplet classes with ten different diameters and five different injection angles. A droplet size distribution measured by Dibelius and Funcke [16] for an identical injection nozzle was used, although this experiment was performed 15 mm downstream of the nozzle. It is assumed that this distribution can be taken as nozzle outlet conditions because no atomization and no break up models were considered.

Further information is summarized in Table 1.

5. RESULTS AND DISCUSSION

5.1. *Penetration length*

An important result of transient spray calculations is the time-dependent axial penetration of a spray within a cylinder. Numerical results are shown in Fig. 2 for the injection of pure *n*-heptane. The boundary conditions are those of Table 1. The agreement with experimental results from spray photographs [17] is acceptable keeping in mind that the spray length strongly depends on the definition of the spray tip position in the numerics as well as in the experiments. The figure indicates that the measured droplet size distribution at 15 mm distance from the nozzle can readily be used as initial conditions and additional atomization, break up, collision and coagulation models can be avoided. Numerical simulations based on break-up models [7,8] resulted in a too short penetration length.

For a detailed discussion of the transport phenom-

Table 1. Initial and boundary conditions

Gas pressure	45 bar	
Initial gas temperature	500°C	
Gas density	19.6 kg m^{-3}	
Injection volume	7 mm^3	
Injection time	1.5 ms	
Nozzle diameter	0.2 mm	
Spray angle	12.5°	
Initial droplet velocity	122–205 m s^{-1}	function of supply pressure history
Initial droplet diameters	2–40 μm	experimental data from ref. [16]
Initial droplet temperature	40°C	

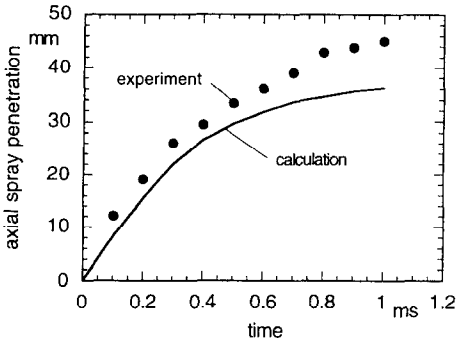

FIG. 2. Axial spray penetration of a single component (*n*-heptane) spray.

ena occuring in sprays with binary liquid fuels the droplet history will first be analysed for single droplets in a large, gaseous atmosphere. In the second part of the presentation sprays will be simulated.

5.2. *Single binary droplets*

Initially, the vaporization of a binary mixture of *n*-heptane and *n*-decane in a stagnant surrounding is investigated. In Fig. 3 the square of the relative droplet diameter is plotted as a function of time. The initial values of temperature, pressure and diameter are 27°C, 1 bar and 1 mm, respectively. These conditions have been chosen because measured data were available by Gökalp [18]. As can been seen the highly volatile *n*-heptane is dominant at the beginning of the vaporization process. After an initial phase the slope of the curve decreases and follows finally the slope of the *n*-decane curve. The agreement with the experiments by Gökalp for an 80%/20%-mixture is satisfactory.

The vaporization curves will be totally different under engine conditions. In Fig. 4 the results for pure *n*-heptane, pure *n*-decane and a 50% *n*-heptane/50% *n*-decane mixture are represented for a droplet of 20 μm initial diameter and an initial temperature of 40°C in stagnant surrounding gas with a temperature of 500°C and a pressure of 45 bar. These values are typically found in engines and will be called standard conditions for the following test cases. In this case a zero velocity of the droplet is assumed. The results of the diffusion limit model (DL) are compared to those of the simple well mixed model (WM) assuming constant temperature and mass fraction along the droplet radius.

As can been seen the droplet diameter increases initially due to thermal expansion. After this heating up phase, which depends on the boiling temperature, the vaporization process dominates and reduces the droplet diameter. The well known linear vaporization curve no longer exists. The vaporization curves for the well mixed model and the diffusion controlled model are very similar, that means that the transport processes within the droplet on the vaporization rate are not very pronounced.

The situation is completely different for high relative velocities between the gas and the droplet resulting in lower heat and mass transfer resistances at the gas side of the droplet surface. The limited heat

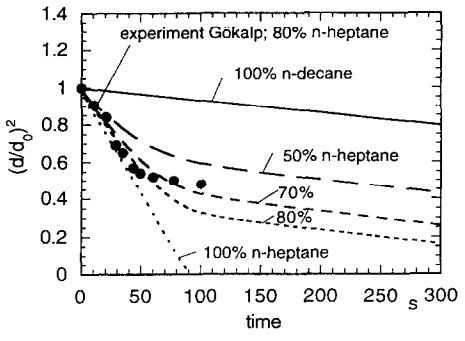

FIG. 3. Vaporization curve for an *n*-heptane/*n*-decane mixture in stagnant surroundings (initial diameter 1 mm, initial temperature 27°C, pressure 1 bar).

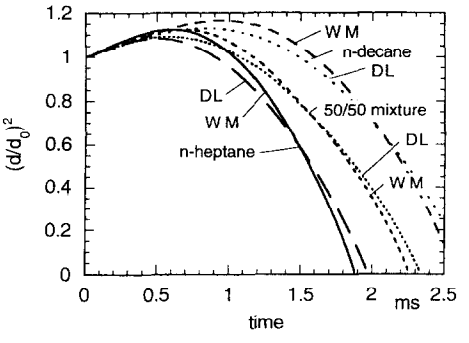

FIG. 4. Vaporization curve for *n*-heptane, *n*-decane and an *n*-heptane/*n*-decane mixture (50%/50%) in a stagnant atmosphere (500°C and 45 bar), initial diameter 20 μm, initial temperature 40°C.

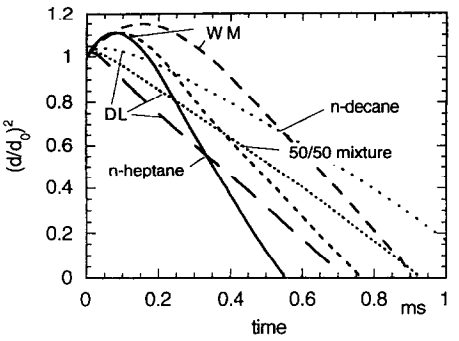

FIG. 5. Vaporization curve for a *n*-heptane/*n*-decane mixture (50%/50%) in a hot atmosphere (500°C and 45 bar); initial diameter 20 μm, initial temperature 40°C, relative initial velocity 100 m s^{-1}.

conduction and the mass diffusion inside the droplet become more important. This case is demonstrated in Fig. 5, where an initial velocity of 100 m s^{-1} is chosen. This value can typically be found near the injection nozzle. The decreasing transient velocity during vaporization is calculated according to the momentum equation (15).

It is interesting to see, that due to the higher initial velocity, the time for complete evaporation is reduced by a factor of three. For pure liquids and for the binary mixture the transport resistances within the droplet increases the vaporization time by 20%. The initial increase of the droplet diameter completely disappears if the transport processes are taken into account.

The effects of the transport limitation can be demonstrated in the following figures. In Fig. 6 the droplet mean temperature for the well mixed model (WM) and the centre, surface and averaged temperatures for the diffusive transport model (DL) are plotted as a function of time for the pure liquids and the binary mixture.

Due to the heat transport resistance the temperature of the outer layer of the droplet increases immediately, whereas the centre of the droplet is still at its initial value. The rapid increase of the surface temperature and the related intensive evaporation at the initial stage explains why the improved droplet model predicts a sharper decrease of the droplet diameter at that stage, see Fig. 5. After a time period of only 0.1 ms the temperature increase in the core of the droplet is higher compared to that of the outer layers. The temperatures never reach their so-called adiabatic values.

In Fig. 7 the corresponding transient values of the *n*-heptane mass fractions are shown for both models.

Analogous to Fig. 6(c) the surface values change rapidly. The *n*-heptane vaporization is very intensive at the beginning. The initial mass fraction of 50% decreases to 20% within 0.2 ms. The core region is still at its initial value at this stage due to the limited mass diffusivity.

The results presented so far demonstrated an

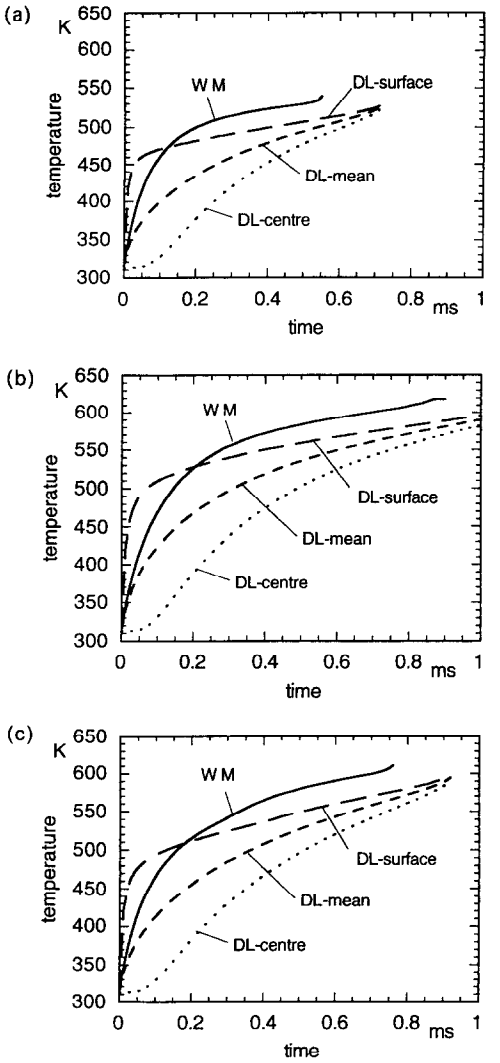

FIG. 6. Transient droplet temperature in a hot atmosphere (500°C and 45 bar), initial diameter 20 μm, initial temperature 40°C, initial relative velocity 100 m s^{-1}. (a) *n*-heptane, (b) *n*-decane, (c) *n*-heptane/*n*-decane mixture (50%/50%).

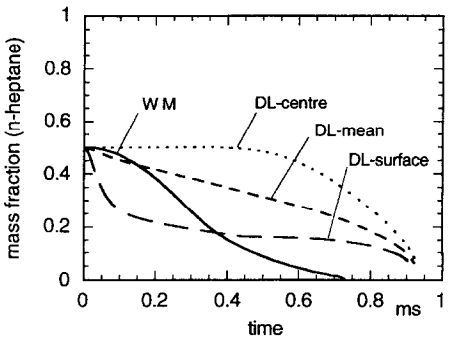

FIG. 7. Transient *n*-heptane mass fraction of an *n*-heptane/*n*-decane (50%/50%) droplet in a hot atmosphere (500°C and 45 bar), initial diameter 20 μm, initial temperature 40°C, initial relative velocity 100 m s^{-1}.

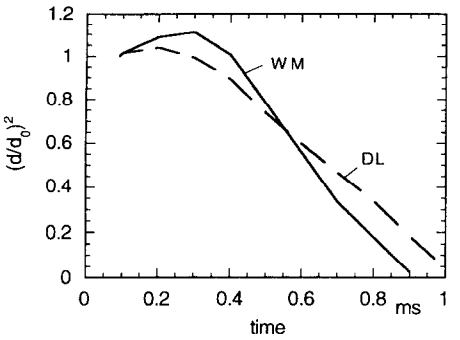

FIG. 8. Vaporization time for a selected droplet with an initial diameter of 23 μm and an injection velocity of 190 m s^{-1}.

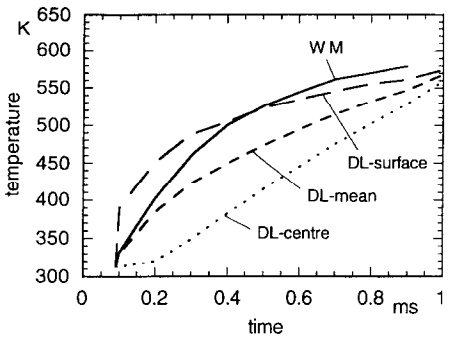

FIG. 9. Transient temperature of a selected droplet with an initial diameter of 23 μm and an injection velocity of 190 m s^{-1}.

important influence of the inner diffusive transport processes for single binary droplets under diesel engine conditions. In the following subsection the numerical simulations will be extended to droplet sprays.

5.3. *Binary droplet sprays*

An important difference between the evaporation of a single droplet and the evaporation of droplet sprays is the interdependence between the transient droplet and the gaseous surrounding. In the case of a transient spray the penetrating droplets will slow down, accelerating the gaseous phase and indirectly the slower smaller droplets. Droplets entering the domain at a later time of injection will meet completely different surroundings, characterized by a higher velocity, lower temperature and increased vapour mass fractions. All these effects are described by the conservation equations (18). The contribution of the present work is to demonstrate the influence of the transport phenomena within the droplets on the spray development and the vaporization rates. Roughly five thousand droplet parcels of the transient spray were tracked within the gas field during an injection time of 1 ms. So it is very difficult to display the numerical results in diagrams for a proper discussion. To allow a comparison with the single droplet calculations shown above droplets with nearly similar diameters were selected from the spray data set and presented in an analogous form.

In Fig. 8 the vaporization rate of a droplet is shown, which leaves the nozzle 0.09 ms after the beginning of the injection. The selected droplet has an initial diameter of 23 μm and an injection velocity of 190 m s^{-1}. The temperature and the pressure of the surrounding gas and the initial liquid temperature are the same as for the single droplet calculations, see Table 1.

The spray predictions should be compared with Fig. 5. It turns out that the vaporization times within the spray are very nearly the same compared to the single droplet calculation although the initial velocity is doubled. As in the case of the single droplet the vaporization time increases by roughly 10% if the internal diffusion processes are considered.

The transient temperature of the selected droplet is presented in Fig. 9. Compared to Fig. 6(c) the final temperatures are lower by 20 K because the surrounding gas is already cooled down by the droplets at the spray tip.

Figure 10 has to be compared with Fig. 7. The transient mass fraction of *n*-heptane is again very similar to the single droplet data. The calculated mean *n*-heptane mass fractions are quite different for both models. Towards the end of the vaporization the mean value of *n*-heptane mass fraction is decreased to 5% for the well mixed model, whereas a value of 30% is predicted for the transport model.

In Figs. 11–13 the influences of the droplet models on the surrounding gas are demonstrated. In Figs. 11 and 12 the profiles of temperature and vapour mass fractions along the spray axis are shown.

After a rapid decrease of the gas temperature within the first 10 mm from the nozzle exit the temperatures increase again due to the mixing with the hot surrounding gas. The gas temperatures predicted by the improved model are roughly 30 K higher, see Fig. 11. As a result of the increased temperature higher vapour mass fractions will be predicted, see Fig. 12. The highly volatile *n*-heptane appears first in the vapour phase of the spray and reaches a maximal value of 6% at a distance of 10 mm, whereas the mass

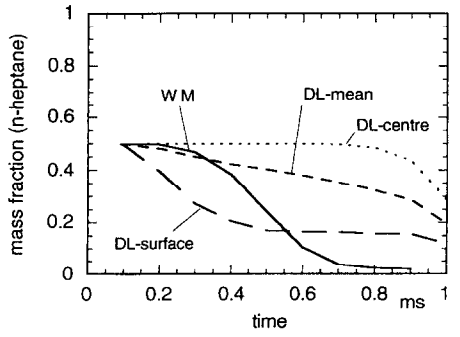

FIG. 10. Transient *n*-heptane mass fraction of a selected droplet with an initial diameter of 23 μm and an injection velocity of 190 m s^{-1}.

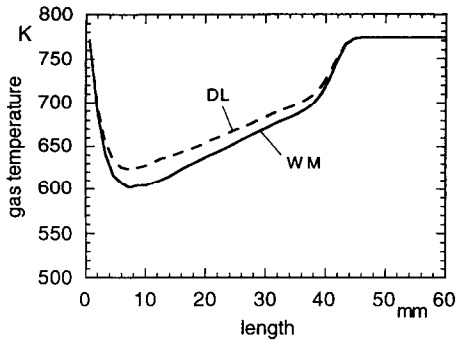

FIG. 11. Axial temperature profile of the gas at the spray axis.

fraction of the low volatile *n*-decane reaches only 4% at a distance of 25 mm.

Typical results of the present spray calculations are summarized in Fig. 13, where the fields of velocity, temperature, and mass fractions of *n*-heptane and *n*-decane are shown for a situation 1 ms after injection. The upper half of the graphs is calculated with the assumption of a well mixed droplet, for the lower half the internal diffusion processes are accounted for. The differences are negligible for the spray penetration and the velocity field, because the momentum transport is not affected by the improved droplet model. The development of the temperature and mass fraction fields is delayed by the diffusion processes within the droplet.

6. CONCLUSION

The present study is concerned with the effect of the internal heat conduction and diffusive mass transport during the vaporization of a binary droplet spray, under conditions which are typical for fuel injection in a diesel engine. The droplet model is an integral part of a general three-dimensional numerical procedure to predict the velocity, temperature and mass fraction fields of the gaseous phase during the transient spray vaporization.

The comparison between computed results using a conventional well mixed droplet model with those

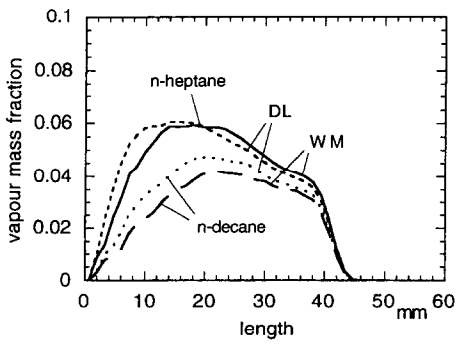

FIG. 12. Axial mass fraction profiles of *n*-heptane and *n*-decane vapour at the spray axis.

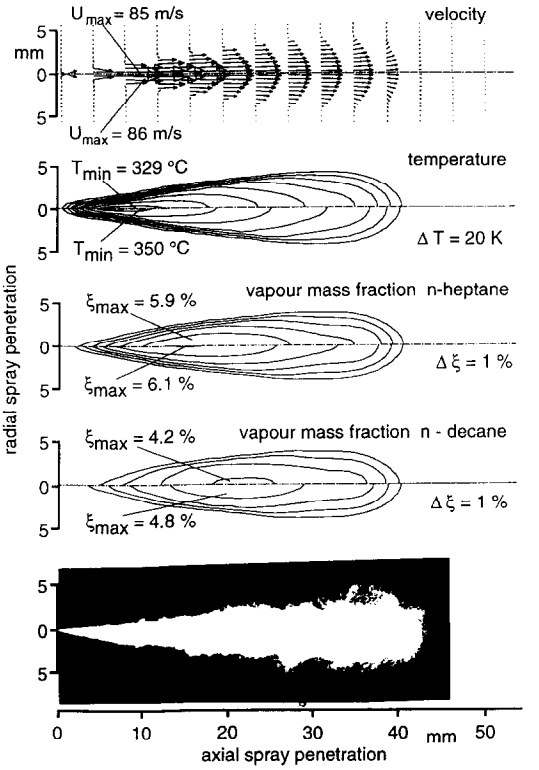

FIG. 13. Velocity, temperature, and species mass fractions of the gas and a spray photograph 1 ms after injection starts (upper part: well mixed model, lower part: diffusion limited model).

from the extended model shows that the influence on the vaporization time is not very pronounced. An increase by only 10–20% of the total vaporization time is predicted if the extended model is used. The predicted penetration of the spray is very similar in both cases and is in agreement with measured data. But important temperature and mass fraction differences within the droplet have been found. There are large differences between the mean values of the droplet temperatures and droplet mass fractions predicted by the conventional model and the averaged values of the extended model during the vaporization process. This is important information for experimentalists using Phase-Doppler-Anemometry to measure droplet size and droplet velocities. Important differences were found in the local mass fraction of the vapour phase too. Because these values are determining the ignition and combustion processes the extended model should be included in general CFD-codes for engine designers. The extra computing time for the extended model within a transient spray calculation as described in the present paper is in the order of 30%.

Acknowledgements—The present study was supported by the Deutsche Forschungsgemeinschaft by a grant from the SFB 224 (Motorische Verbrennung). The extended droplet model is mainly based on the work of the Institut für Thermische Strömungsmaschinen, Universität Karlsruhe. This support is gratefully acknowledged.

REFERENCES

1. G. M. Faeth, Evaporation and combustion of sprays, *Prog. Energy Combust. Sci.* **9,** 1–76 (1983).
2. W. A. Sirignano, An integrated approach to spray combustion model development, *Combust. Sci. Tech.* **58,** 231–251 (1988).
3. C. K. Law, Recent advances in droplet vaporization and combustion, *Prog. Energy Combust. Sci.* **8,** 171–201 (1982).
4. SPEED-code, developed by D. Gosman, Department of Mechanical Engineering, Imperial College London, within the CEC programme JRC-IDEA (1993).
5. FIRE-code, developed by AVL, Graz, Austria (1993).
6. F. Obermeier, MPI für Strömungsforschung, Göttingen, Model development within the CEC programme JRC-IDEA (1993).
7. A. A. Amsden, P. J. O'Rourke and T. D. Butler, KIVA II: A computer program for chemically reactive flows with sprays, Los Alamos Report LA-11560-MS (1989).
8. J. Anders and J. Karlsson, The SPICE-code for prediction of spray ignition, combustion and emission, Dept. of Thermo- and Fluid Dynamics, Chalmers University of Technology, Göteborg, Sweden (1991).
9. R. Kneer, M. Schneider, B. Noll and W. Wittig, Diffusion controlled evaporation of a multicomponent droplet: theoretical studies on the importance of variable liquid properties, *Int. J. Heat Mass Transfer* **36,** 2403–2415 (1993).
10. P. L. Lage, C. M. Hackenberg and R. H. Rangel, Non-ideal vaporization of dilating binary droplets with variable properties, *Int. J. Heat Mass Transfer* **36,** 3731–3741 (1993).
11. S. K. Aggarwal and G. Chen, Vaporization behavior of fuel droplets in a hot air stream, *Int. J. Heat Mass Transfer* **34,** 2669–2673 (1991).
12. K. Annamalai, W. Ryan and S. Chandra, Evaporation of multicomponent drop arrays, *J. Heat Transfer* **115,** 707–716 (1993).
13. M. Renksizbulut, M. Bussmann and X. Li, A droplet vaporization model for spray calculations, *Par. Part. Syst. Charact.* **9,** 59–65 (1992).
14. T. L. Jiang and W. T. Chiang, Effect of multiple droplet interaction on droplet vaporization in subcritical and supercritical pressure environments, accepted for publication, *Combust. Flame* (1994).
15. FLUENT Inc., Centerra Resource Park, Lebanon, HH, 03766, U.S.A.
16. G. Dibelius and J. Funcke, Zerstäubung des Kraftstoffstrahls und Tropfenverdampfung bei der dieselmotorischen Einspritzung, Kolloquium des Sonderforschungsbereichs SFB 224, Motorische Verbrennung, RWTH Aachen, pp. 248–272, 6, 7 October (1988).
17. U. Renz, A. Breuer and M. Klingsporn, Strahlausbreitung und Tropfenverdampfung bei der dieselmotorischen Einspritzung, Kolloquium des Sonderforschungsbereichs SFB 224, Motorische Verbrennung, RWTH Aachen, 11, 12 March (1993).
18. I. Gökalp, C.R.C.C.H.T.-C.N.R.S, Orleans, France, Experiments presented within a workshop organized by the CEC programme JRC-IDEA (1992).
19. R. C. Reid, J. M. Prausnitz and B. E. Poling, *The Properties of Gases and Liquids* (4th Edn). McGraw-Hill, New York (1987).
20. A. S. Teja, Simple method for the calculation of heat capacities of liquid mixtures, *J. Chem. Engng Data* **28,** 83–85 (1983).
21. R. C. Reid, J. M. Prausnitz and B. E. Poling, *The Properties of Gases and Liquids* (3rd Edn). McGraw-Hill, New York (1977).
22. T. E. Daubert and R. P. Danner, Physical and thermodynamic properties of pure chemicals: data compilation. Hemisphere, New York (1989).
23. T. P. Coffee and J. M. Heimerl, Transport algorithms for premixed, laminar steady-state flames, *Combust. Flame* **43,** 273–289 (1981).
24. R. B. Bird, W. E. Stewart and E. N. Lightfoot, *Transport Phenomena*. Wiley, New York (1960).

APPENDIX

Thermophysical properties

Liquid phase. The properties of the liquids are calculated using reduced temperatures in order to get reasonable values also near the critical temperature. The liquid density is determined through the modified Rackett equation [19] using the mixing rule of Chueh and Prausnitz [19]. The specific heat is calculated by the Rowlinson–Bondi equation [19] with a mixing law proposed by Teja [20] for hydrocarbons assuming a mass mean average at the same reduced temperatures. The liquid thermal conductivity is predicted by the method of Latini and the mixing rule of Baroncini [19]. The binary diffusion coefficient is determined by the method of Lusis *et al.* [21], using the dynamic viscosity calculated through the equation of Van Velzen *et al.* [19]. The activity and fugacity coefficients are set equal to one, assuming ideal liquid and gas phase behaviour. Most of the constants are taken from Reid *et al.* [19] and Daubert and Danner [22], as well as the equations for vapour pressure and heat of vaporization.

Gaseous phase. The gas phase properties, to be used in the heat, mass and momentum correlations are calculated using the 1/3-rule for temperature and mass fraction. The gas density and specific heat capacity are determined by assuming ideal gas behavior. The viscosity is determined by Wilke's method [19] and the thermal conductivity is calculated using the mixing rule of Coffee and Heimerl [23]. The binary diffusion coefficients are predicted by the method of Fuller *et al.* [19] and the effective diffusion coefficient by Bird *et al.* [24]. The equations for the data of the pure components are based on experimental data and can be found in ref. [22]. The influence of pressure is taken into account for density and diffusion coefficient.